 doi:10.20944/preprints201806.0328.v1

Mechanical Properties of Ti-alloy joint with $Ti_{20}Zr_{20}Cu_{60-x}Ni_x$ (x = 10, 20, 30, 40 and 50) filler metal

P. Rama Rao*[1, 3], Bhaskar. Majumdar[2] and Anil. K. Bhatnagar[1]

[1] *School of Engineering Sciences & Technology*
University of Hyderabad, Hyderabad 500046, India
[2] *Defence Metallurgical Research Laboratory (DMRL)*
Kanchanbagh, Hyderabad – 500058, India
[3]*CSIR-Central Glass and Ceramic Research Institute, Kolkata – 700032, India*

(*corresponding author: ramarao@cgcri.res.in)

Abstract: The developed microstructure features a long with mechanical properties in vacuum brazing of commercially pure Ti-alloy using $Ti_{20}Zr_{20}Cu_{60-x}Ni_x$ (x=10, 20, 30, 40 and 50) metallic filler. Brazing temperatures and holding times employed in this study were 1240-1279 K (967-1006^{o}C) for a period of 10 min, respectively. The mechanical properties of brazed joints were evaluated by nanoindention at a constant peak load of 5000 μN and tensile tests. The number of intermetallic phase, such as $NiTi_2$, Ti_2Cu, $(Ti, Zr)_2Cu$, $(Ti, Zr)_2Ni$, β(Ti, Zr), α-Ti and NiTi. The solid solution matrix have been identified at 1279 K out of these different regions the $NiTi_2$ rich region had the highest nanohardness of 17 GPa, It is interesting to note that among five different glasses, the $Ti_{20}Zr_{20}Cu_{10}Ni_{50}$ has the highest yield strength of 17 GPa, which is mainly due to $NiTi_2$ phase. Based on the tensile test results all cracks propagate along the brittle intermetallic compounds like $NiTi_2$ in the reaction layer the reduction of the strength of the joints and fracture behaviour upon propagation of the crack, which shows the morphological cleavage including facets characteristics.

Keywords: Vacuum brazing, metallic glasses, Ti-alloy, Mechanical properties.

Preprints (www.preprints.org) | NOT PEER-REVIEWED | Posted: 21 June 2018 doi:10.20944/preprints201806.0328.v1

1. INTRODUCTION

The metallic amorphous alloys were widely studied in the recent past because they possess excellent characteristics *viz*., soft magnetic properties, greater compressive strength and significant behaviour of anti-corrosion. There were first report of high glass forming ability (GFA) of Cu-Ti based alloys namely, $Cu_{47}Ti_{34}Zr_{11}Ni_8$ and $Cu_{47}Ti_{33}Zr_{11}Ni_8Si_1$, which can be cast fully amorphous in the rod forms of 4 and 7 mm in diameter [1-5]. Afterwards, much effort were made in order to develop novel Cu-Ti based bulk glassy alloys possessing more GFA and improved mechanical properties [6, 7]. However, it has been observed that the metallic glasses have drawbacks which are the lack of ductility shown in tensile experiments and limited plasticity under macroscopic compression. Therefore, in order to overcome the above constraints, the technique of the nanoindentation has become popular to evaluate mechanical properties of these materials [8-10]. The response of nanoindentation on Cu-Ti based metallic glasses has recently been appeared [11]. Electrical resistivity is also an important parameter, which is necessary to assess the characteristics of these metallic glasses. The variations of the physical, mechanical and electrical properties of $Ti_{20}Zr_{20}Cu_{60-x}Ni_x$ (x=10, 20, 30, 40 and 50) metallic glasses as a function of composition are discussed in this Paper.

2. EXPERIMENTAL METHODS

The alloy with nominal composition $Ti_{20}Zr_{20}Cu_{60-x}Ni_x$ (x=10, 20, 30, 40 and 50) is prepared from pure elements (purity > 99.9 wt. %) by arc melting in a titanium-gettered argon atmosphere. For achieving homogeneity in the alloy composition, it is remelted many times. The amorphous ribbon of this compound is prepared using the standard rapid quenching technique. The ribbon is about 25 mm wide and 100 μm thick. The Field Emission Gun (FEG) is usually a wire of Tungsten (W) Zigma, Carl Zeiss, Germany (FE-SEM, Carl ZEISS, FEG andUltra 55), 30kV, images were obtained at an operating voltage of 15 kV and the working distance was about 8.5

Preprints (www.preprints.org) | NOT PEER-REVIEWED | Posted: 21 June 2018 doi:10.20944/preprints201806.0328.v1

mm. The nano-mechanical properties such as hardness and Young's modulus were determined using a Hysitron Nanomechanical system (Tribo Indentor, 900 series, USA). The machine had depth resolution of 0.04nm and load resolution of 1nN. The thermal drift was kept to <0.5nm/s. The machine had a load range of 1 to 10,000 μN. The Berkovich indenter used in all the nanoindentation experiments had a tip radius of about 120 nm and a semi-apex angle of 65.3°. The samples were indented with a maximum load of 5000μN. The trapezoid load function (which includes the loading, holding and unloading segments) was used to measure the hardness of the ribbons and lap joint samples with a loading rate of 200 μNs^{-1}, segment time of 10s and dwell time of 10s.

Vacuum brazing was performed to braze commercially pure CP-Ti plates using the as spun $Ti_{20}Zr_{20}Cu_{60-x}Ni_x$ (x=10, 20, 30, 40 and 50) metallic glass ribbon as filler material. The 1.5 mm thick commercial pure Ti was used in this work, which has been transformed to β-phase after furnace cooling from 1263 K. The chemical composition (wt.%) of the base metal *viz*., C, O, Fe, N, H and Ti are 0.1, 0.2, 0.08, 0.15, 0.01 and balance amount, respectively [12]. The parent metal pieces were polished first with SiC papers up to 600-1200 grade and cleaned subsequently by an ultrasonic bath with acetone for 20 min at 50^{o}C prior to insertion in the furnace for brazing. After cleaning the brazing foils with acetone and afterwards they were sandwiched between the merging areas of the native metals. The first lap shear metal specimen of 8.16 and 14.18 mm width and length, respectively with decreased cross-section was brazed with 4.5 mm overlapping using wire cutting machine electrical discharge machine EDM, model JISZ 3192.

Tensile tests of the brazed joints both at room temperature were carried out at a constant speed of 0.5 mm/min by a universal testing machine UTM (INSTRON 5500R). The machine had load cells of 1 and 100kN with an accuracy of ±1% of full scale.

Preprints (www.preprints.org) | NOT PEER-REVIEWED | Posted: 21 June 2018 doi:10.20944/preprints201806.0328.v1

3. RESULTS AND DISCUSSION

3.1 The nanoindentation studies on the $Ti_{20}Zr_{20}Cu_{60-x}Ni_x$ (x=10, 20, 30, 40 and 50) metallic glasses.

The typical representative P-h plots measured at a load of 5,000 mN for the metallic glasses (a) $Ti_{20}Zr_{20}Cu_{50}Ni_{10,}$ (b) $Ti_{20}Zr_{20}Cu_{40}Ni_{20,}$ (c) $Ti_{20}Zr_{20}Cu_{30}Ni_{30,}$ (d) $Ti_{20}Zr_{20}Cu_{20}Ni_{40}$ and (e) $Ti_{20}Zr_{20}Cu_{10}Ni_{50}$ are shown in Figs 1 (a), (b), (c), (d) and (e), respectively. Based on these data and using the mathematical formalism of the Oliver and Pharr model [13-15], as described earlier in chapter 2, the nanohardness (H) and the reduced Young's modulus (E) were estimated. All these data are depicted in Table 1. The data presented in Table 1 show that both reduced Young's modulus (E) and nanohardness (H) increased approximately linearly as the Ni percentage was increased from 10 to 50% in the corresponding compositions. The reason for this is yet to be well understood and hence further work will need to be done in future to understand the genesis of this behaviour.

Table 1 Calculated values of hardness and Young's modulus of $Ti_{20}Zr_{20}Cu_{60-x}Ni_x$ (x=10, 20, 30, 40 and 50) metallic glasses measured at a load of 5000 μN

Composition	Calculated values of hardness and Young's modulus as-spun ribbons	
	E (GPa)	H (GPa)
Ti_{20} Zr_{20} Cu_{50} Ni_{10}	107	7.0
Ti_{20} Zr_{20} Cu_{40} Ni_{20}	112	6.9
Ti_{20} Zr_{20} Cu_{30} Ni_{30}	121	7.2
Ti_{20} Zr_{20} Cu_{20} Ni_{40}	122	7.3
Ti_{20} Zr_{20} Cu_{10} Ni_{50}	124	7.4

Preprints (www.preprints.org) | NOT PEER-REVIEWED | Posted: 21 June 2018 doi:10.20944/preprints201806.0328.v1

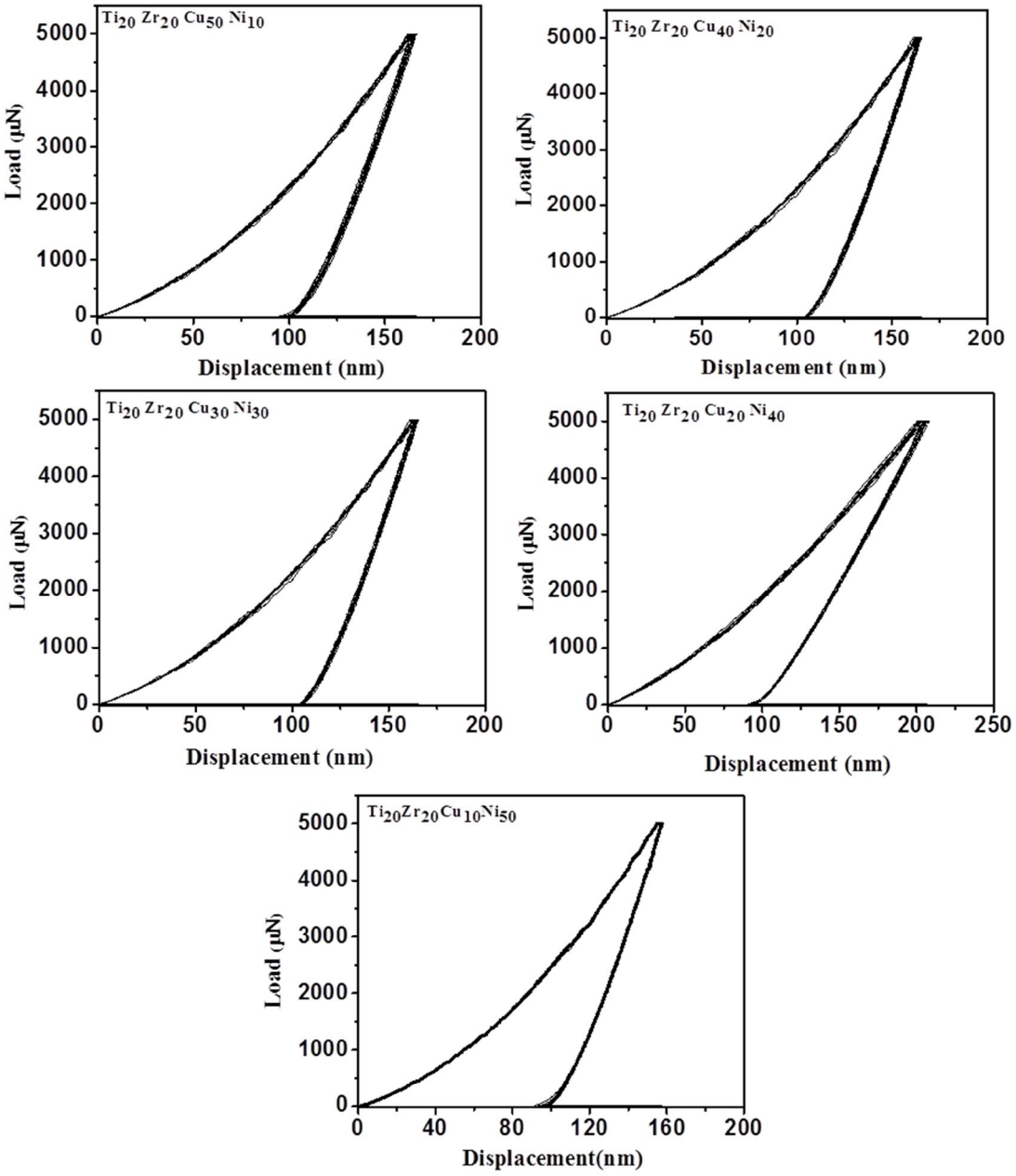

Fig. 1 The typical representative P-h plots measured at a load of 5000 μN for the metallic glasses (a) $Ti_{20}Zr_{20}Cu_{50}Ni_{10,}$ (b) $Ti_{20}Zr_{20}Cu_{40}Ni_{20,}$ (c) $Ti_{20}Zr_{20}Cu_{30}Ni_{30,}$ (d) $Ti_{20}Zr_{20}Cu_{20}Ni_{40}$ and (e) $Ti_{20}Zr_{20}Cu_{10}Ni_{50}$.

Preprints (www.preprints.org) | NOT PEER-REVIEWED | Posted: 21 June 2018 doi:10.20944/preprints201806.0328.v1

4. Nanoindentation for brazed samples

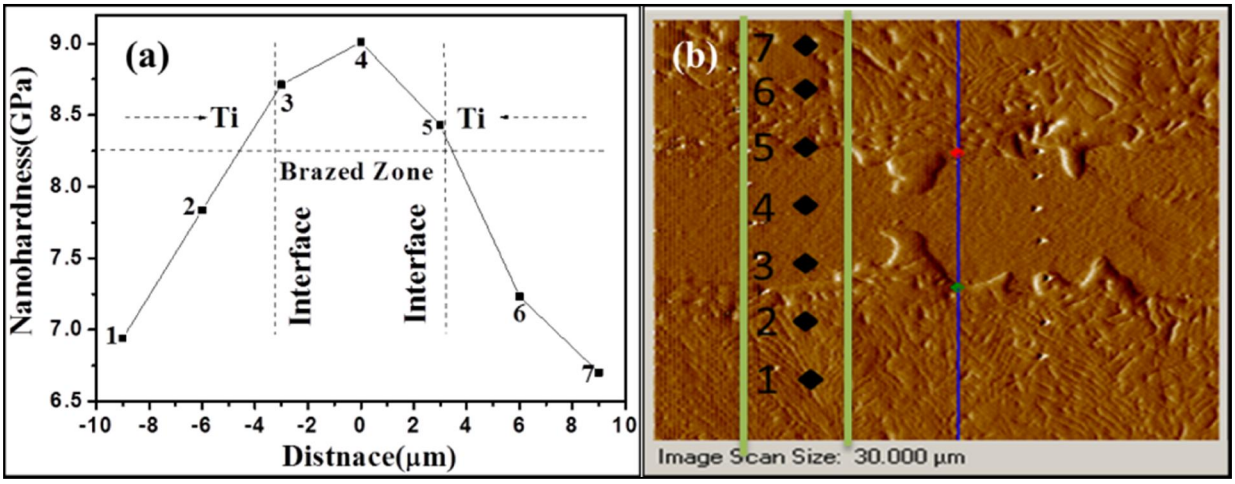

Fig. 2 Nanohardness of Ti/$Ti_{20}Zr_{20}Cu_{50}Ni_{10}$/Ti joint brazed at 1263 K for period of 10 min: (a) Nanohardness profile as a function of distance from 10 μm on both sides of the microstructure through the brazed joint and (b) SPM images of the corresponding nanoindents at different regions of the microstructure of the brazed joint.

The appearance of a microstructure of Ti_2Cu and $NiTi_2$ precipitations surrounded by $Ti_{20}Zr_{20}Cu_{50}Ni_{10}$ solid solution matrix was due to brazing at 1263 K for a period of 10 min. The corresponding nanohardness profile as a function of distance particularly from 10 μm on both sides of the microstructure during brazed joint and SPM images of the nanoindent at different regions of the microstructure of the brazed joint are indicated in Figs.2 (a) and (b), respectively. In Fig. 2 (b), the microstructure contained $(Ti, Zr)_2Cu$, Ti_2Cu and $NiTi_2$ and Ti-rich portions marked as regions 3,4 and 5, respectively [16-18]. However, the eutectoid phase rich portions marked as regions 1, 2, 6 and 7 which are lying on outer side of the brazed joint.

Thus, the portions marked as regions 3, 4 and 5 in Figure 2(b) were inside the brazed joint. Out of these different regions the Ti_2Cu and $NiTi_2$ intermetallic rich portion marked as region 4 had the highest nanohardness of 9 GPa, Fig. 2(a). The $(Ti, Zr)_2Cu$ rich portion marked as region 3 had the next highest nanohardness of about 8.7 GPa, as indicated in Fig. 2(a). The Ti-rich portion

Preprints (www.preprints.org) | NOT PEER-REVIEWED | Posted: 21 June 2018 doi:10.20944/preprints201806.0328.v1

marked as region 5 had a nanohardness of about 8.2 GPa (see Fig.2a). Again, depending on the local eutectoid phase compositions as shown in Fig. 2(a); the nanohardness varied from low as about 6.7 GPa in region 7 to as high as about 7.8 GPa in region 2.

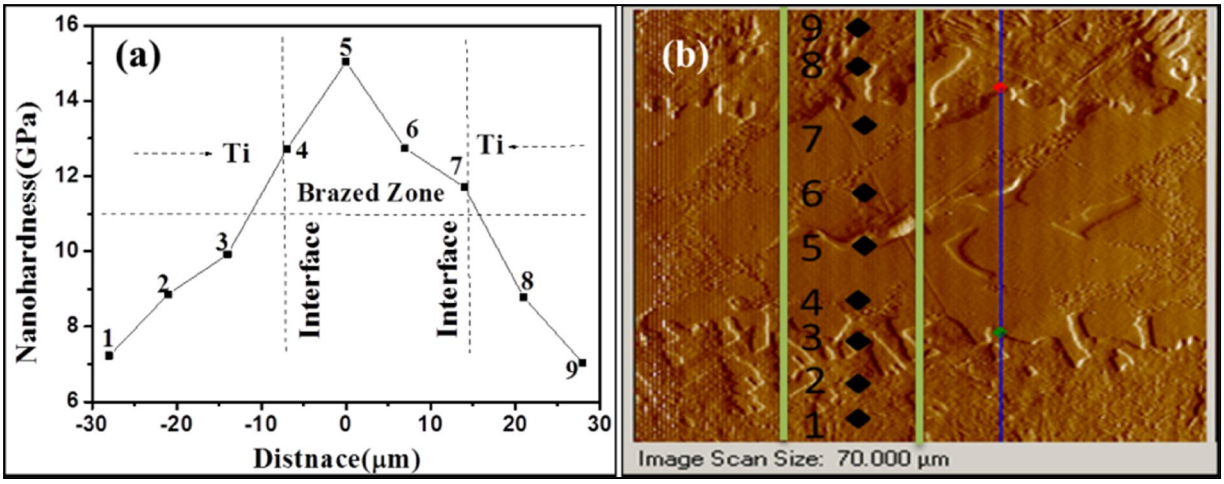

Fig.3 Nanohardness of Ti/$Ti_{20}Zr_{20}Cu_{40}Ni_{20}$/Ti joint brazed at 1240 K for period of 10min: (a) Nanohardness profile as a function of distance from 10 μm on both sides of the microstructure through the brazed joint and (b) SPM images of the corresponding nanoindent at different regions of the microstructure of the brazed joint.

In Fig. 3 (b), the microstructure obtained α-Ti, Ti_2Cu, $NiTi_2$ and β-Ti marked as regions 3, 4, (5 and 6) and 7, respectively, whereas Ti-rich portions are marked as regions 1,2, 8 and 9 lying outside the brazed joint. Thus, the portions marked as regions 3, 4 and 5 in Fig. 3(b) were inside the brazed joint. Out of these different regions the Ti_2Cu rich region 4 had the 3rd highest nanohardness of 12.6 GPa, the $NiTi_2$ rich region 5 had the highest nanohardness of 15 GPa, and the Ti_2Cu rich region 6 had the 2nd highest nanohardness of 13.4 GPa. Further, the α-Ti rich region 3 had a slightly lower nanoharness of 10 GPa. Brazing developed a thin layer of β-Ti between the basemetal and reaction layers. A slightly higher nanohardness of 11.8 GPa was recorded in the β-Ti rich region 7. On the other hand, the Ti rich regions 1, 2, 8 and 9 had much lower nanohardness of only about 6-8 GPa.

Preprints (www.preprints.org) | NOT PEER-REVIEWED | Posted: 21 June 2018 doi:10.20944/preprints201806.0328.v1

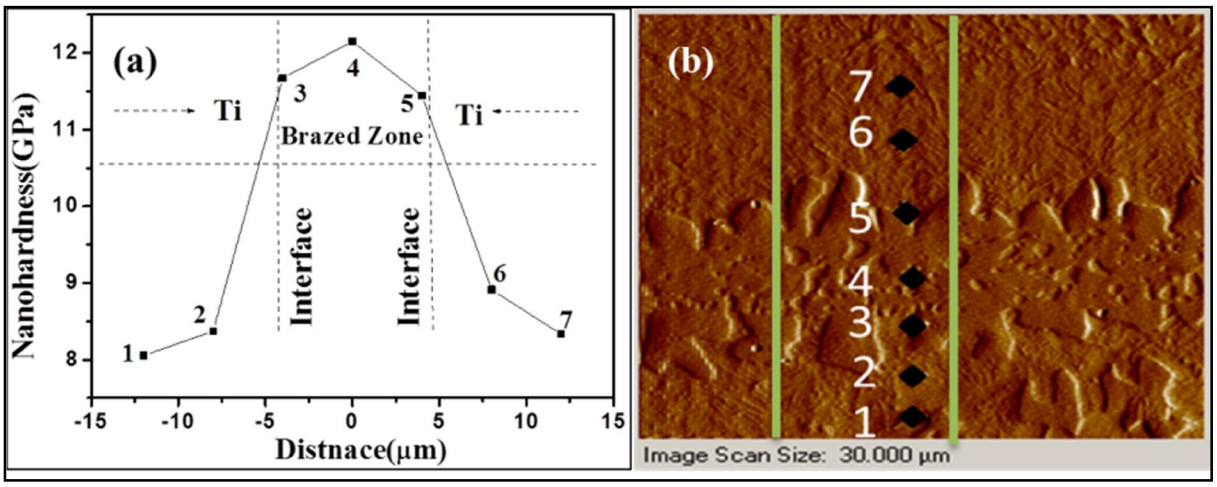

Fig.4 Nanohardness of Ti/$Ti_{20}Zr_{20}Cu_{30}Ni_{30}$/Ti joint brazed at 1268 K for period of 10min: (a) Nanohardness profile as a function of distance from 10 μm on both sides of the microstructure through the brazed joint and (b) SPM images of the corresponding nanoindents at different regions of the microstructure of the brazed joint.

Similarly, in Fig 4 (b), the microstructure contained the Ti-rich portions are marked as regions 1, 2, 6 and 7 lying outside the brazing zones, the α-Ti, Ti_2Cu and $(Ti,Zr)_2Ni$ rich portions are marked as regions 3,4 and 5, respectively, which are inside the brazing zones. Out of these different regions the Ti_2Cu rich region 4 had the highest nanohardness of 12 GPa, the $(Ti,Zr)_2Ni$ rich region 5 had the 2^{nd} highest nanohardness of 11.4 GPa, and the a-Ti rich region 3 had the 2^{nd} highest nanohardness of 11GPa. On the other hand, the Ti rich regions 1, 2, 6 and 7 had much lower nanohardness of only about 8 GPa.

Preprints (www.preprints.org) | NOT PEER-REVIEWED | Posted: 21 June 2018 doi:10.20944/preprints201806.0328.v1

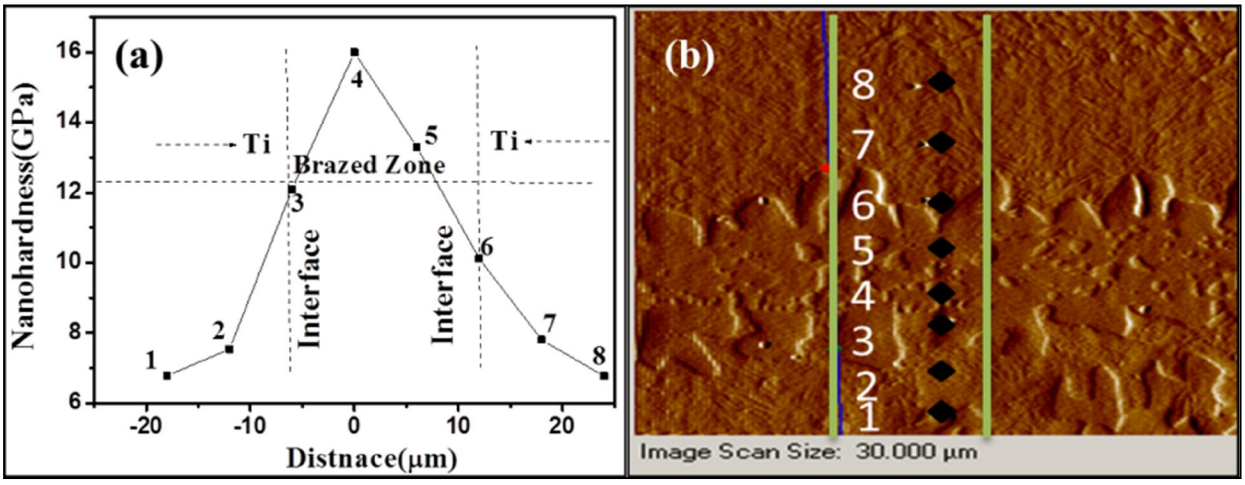

Fig.5 Nanohardness of Ti/$Ti_{20}Zr_{20}Cu_{20}Ni_{40}$/Ti joint brazed at 1277 K for period of 10min: (a) Nanohardness profile as a function of distance from 10 μm on both sides of the microstructure through the brazed joint and (b) SPM images of the corresponding nanoindents at different regions of the microstructure of the brazed joint.

In Fig 5 (b), the microstructure contained the Ti-rich portions are marked as regions 1, 2, 7 and 8 lying outside the brazing zones, the β (Ti, Zr), $NiTi_2$ and $(Ti, Zr)_2Ni$ rich portions are marked as regions 3,4 and 5, respectively, which are inside the brazing zones, while the Ti-rich region 6 is outside the brazing zone. Out of these different regions the $NiTi_2$ rich region 4 had the highest nanohardness of 16 GPa, the $(Ti, Zr)_2Ni$ rich region 5 had the 2^{nd} highest nanohardness of 13GPa, and the β (Ti, Zr) rich region 3 had the 3^{rd} highest nanohardness of 12 GPa. On the other hand, the Ti rich regions 1, 2, 6 and 7 had much lower nanohardness of only about 6-7 GPa.

Preprints (www.preprints.org) | NOT PEER-REVIEWED | Posted: 21 June 2018 doi:10.20944/preprints201806.0328.v1

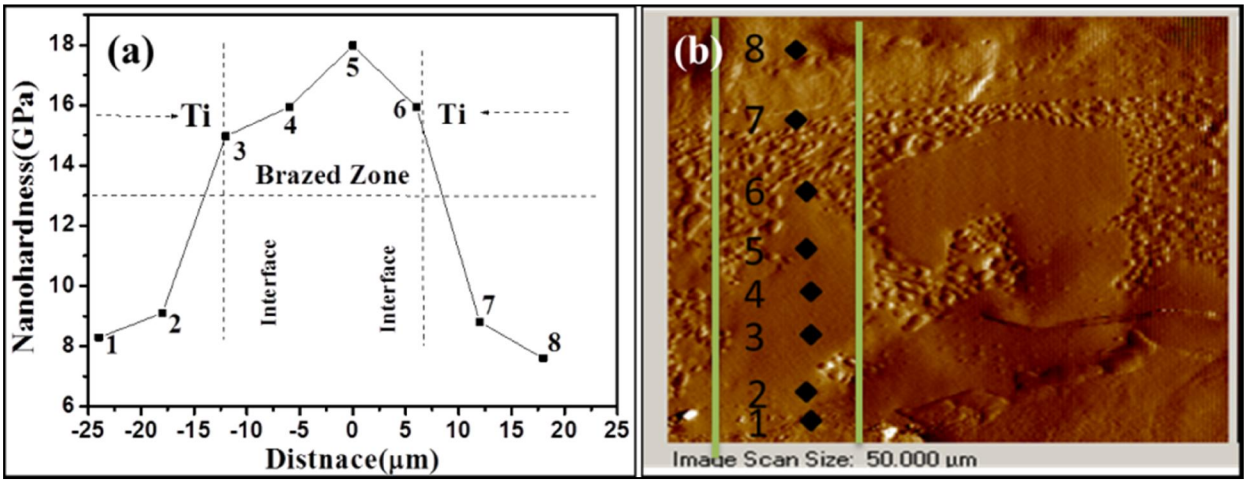

Fig.6 Nanohardness of Ti/$Ti_{20}Zr_{20}Cu_{10}Ni_{50}$/Ti joint brazed at 1279 K for period of 10min: (a) Nanohardness profile as a function of distance from 10 μm on both sides of the microstructure through the brazed joint and (b) SPM images of the corresponding nanoindents at different regions of the microstructure of the brazed joint.

The similar trend has also been observed in Ti/$Ti_{20}Zr_{20}Cu_{10}Ni_{50}$/Ti brazed joint metallic glass (Fig 6 (b)). In Fig 6 (b), the microstructures of the Ti rich portions are marked as regions 1, 2, 7 and 8 lying outside the brazing zone, the α–Ti, NiTi, $NiTi_2$ and Cu_2(Ni, Zr) rich portions are marked as regions 3, 4, 5 and 6, respectively, which are inside the brazing zones. Out of these different regions the $NiTi_2$ rich region 5 had the highest nanohardness of 17 GPa, the Cu_2(Ni,Zr) rich region 6 and the NiTi rich region 4 had the 2nd highest nanohardness of 15.8 GPa, and the α-Ti rich region 3 had the 3rd highest nanohardness of 14.8 GPa. On the other hand, the Ti rich regions 1, 2, 7 and 8 had much lower nanohardness of only about 7-8 GPa [19-25].

Preprints (www.preprints.org) | NOT PEER-REVIEWED | Posted: 21 June 2018 doi:10.20944/preprints201806.0328.v1

5. Butt-lap joints tensile strength characterization

During the tensile strength experiment of the Ti/$Ti_{20}Zr_{20}Cu_{50}Ni_{10}$/Ti brazed joint at 1263 K for a period of 10 min in butt-lap joint, the load against tensile extension plot and FESEM fracture surface image are indicated in Figs. 7 (a) and (b), respectively [26]. True stress at maximum load was only 50.97 MPa because it had a low yield strength corresponding to a low nanohardness of 9 GPa. This was due to the microstructure of Ti_2Cu and $NiTi_2$ complex formation around the solid solution matrix of $Ti_{20}Zr_{20}Cu_{50}Ni_{10}$. Fig.7 (b) demonstrates a typical brittle rupture, which was characterized by the cleavage of high facets with river markings. Similar observations were made in all the metallic glasses Figurs7b-11b.

Similarly, the behaviours of tensile extension plot and FESEM images of Ti/$Ti_{20}Zr_{20}Cu_{40}Ni_{20}$/Ti, Ti/$Ti_{20}Zr_{20}Cu_{30}Ni_{30}$/Ti, Ti/$Ti_{20}Zr_{20}Cu_{20}Ni_{40}$/Ti and Ti/$Ti_{20}Zr_{20}Cu_{10}Ni_{50}$ /Ti brazed joints at different temperatures for a period of 10 min are given in Figs. 7-11, respectively. The corresponding true stresses at maximum load for the above brazing joints are given in Table 2. The corresponding higher yield strengths are due to higher nanohardness, which are 9, 15, 12, 16 and 17 GPa for the five brazed joint metallic glasses mentioned above. The microstructures are due to the complex formation around above mentioned brazed joint glasses of the solid solution matrices. It is interesting to note that among five different glasses, the $Ti_{20}Zr_{20}Cu_{10}Ni_{50}$ has the highest yield strength of 17 GPa, which is mainly due to $NiTi_2$ phase [27-29].

Preprints (www.preprints.org) | NOT PEER-REVIEWED | Posted: 21 June 2018 doi:10.20944/preprints201806.0328.v1

Table 2 The tensile test results for brazed joint samples.

Composition	Brazed Temp.(K)	Maximum Load (N)	True stress at Maximum Load (MPa)
Ti_{20} Zr_{20} Cu_{50} Ni_{10}	1263	5.6	50.97
Ti_{20} Zr_{20} Cu_{40} Ni_{20}	1240	6.4	63.84
Ti_{20} Zr_{20} Cu_{30} Ni_{30}	1268	6.6	60.01
Ti_{20} Zr_{20} Cu_{20} Ni_{40}	1277	5.3	50.61
Ti_{20} Zr_{20} Cu_{10} Ni_{50}	1279	6.3	65.87

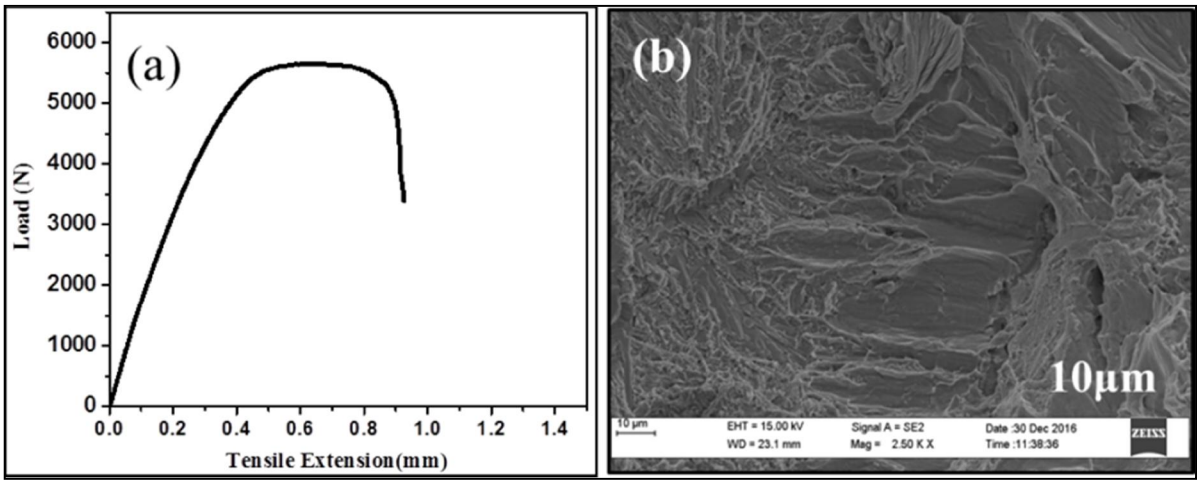

Fig.7 Tensile test data of Ti/$Ti_{20}Zr_{20}Cu_{50}Ni_{10}$/Ti brazed joint at 1263 K for a period of 10 min: (a) Load versus tensile extension plot and (b) FESEM image of fracture surface.

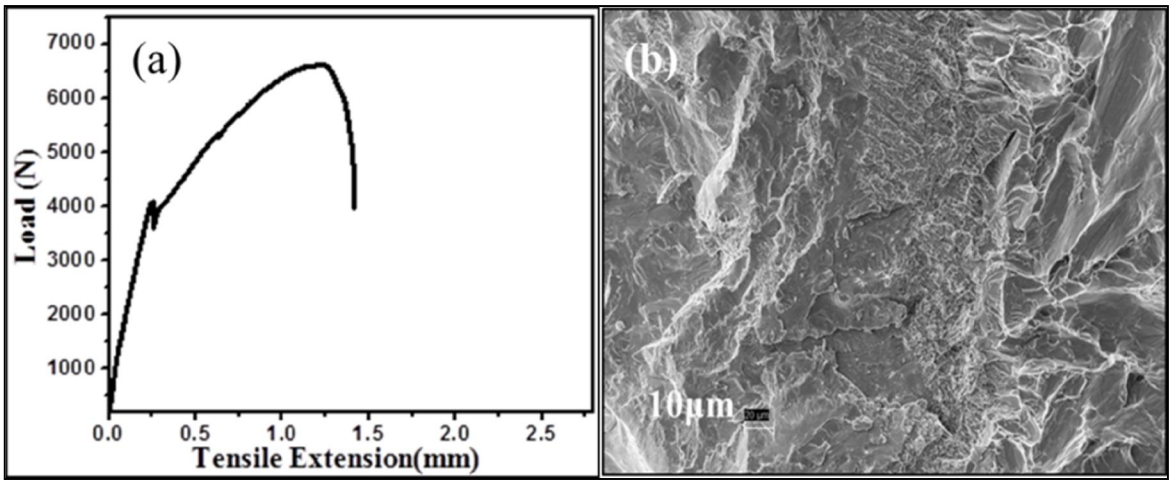

Fig.8 Tensile test data of Ti/$Ti_{20}Zr_{20}Cu_{40}Ni_{20}$/Ti brazed joint at 1240 K for a period of 10 min: (a) Load versus tensile extension plot and (b) FESEM image of fracture surface.

Preprints (www.preprints.org) | NOT PEER-REVIEWED | Posted: 21 June 2018 doi:10.20944/preprints201806.0328.v1

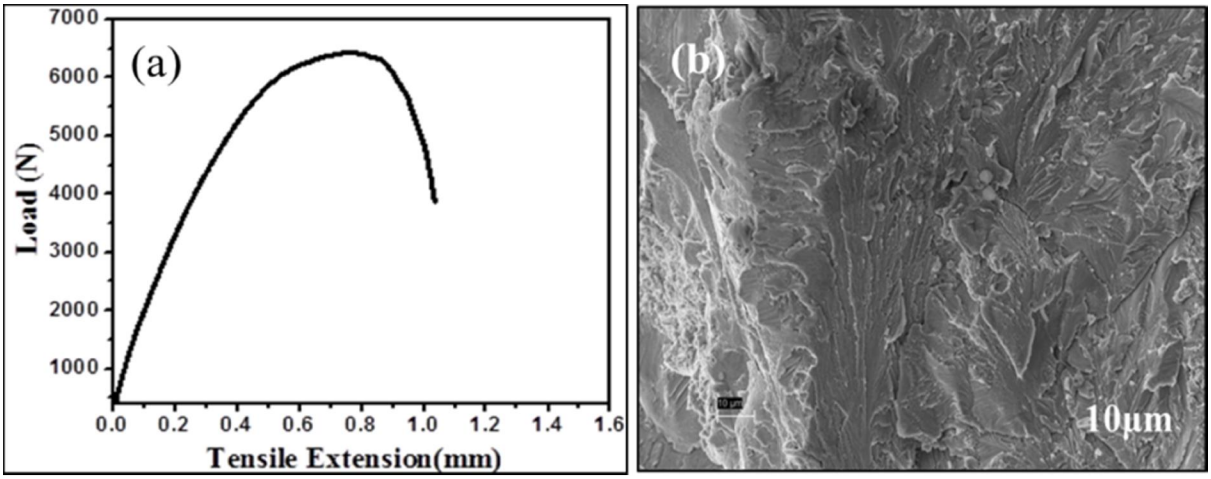

Fig.9 Tensile test data of Ti/$Ti_{20}Zr_{20}Cu_{30}Ni_{30}$/Ti brazed joint at 1268 K for a period of 10 min: (a) Load versus tensile extension plot and (b) FESEM image of fracture surface.

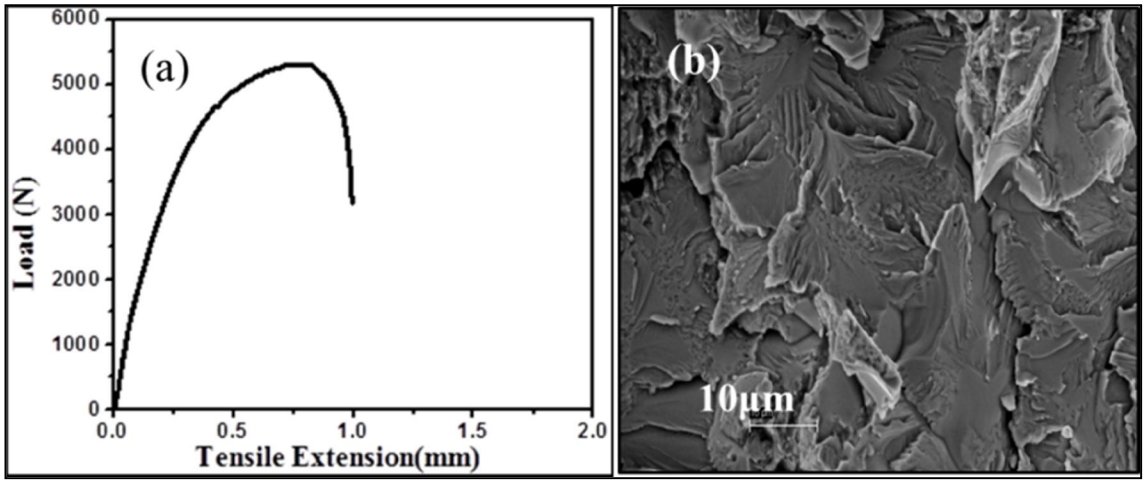

Fig.10 Tensile test data of Ti/$Ti_{20}Zr_{20}Cu_{20}Ni_{40}$ /Ti brazed joint at 1277 K for a period of 10 min: (a) Load versus tensile extension plot and (b) FESEM image of fracture surface.

Preprints (www.preprints.org) | NOT PEER-REVIEWED | Posted: 21 June 2018 doi:10.20944/preprints201806.0328.v1

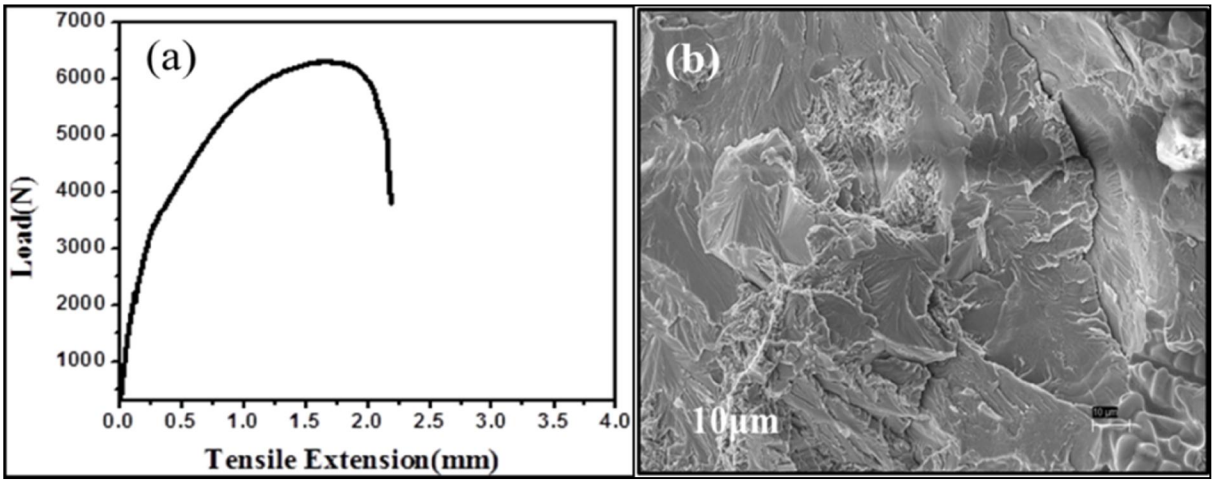

Fig.11 Tensile test data of Ti/$Ti_{20}Zr_{20}Cu_{10}Ni_{50}$/Ti brazed joint at 1279 K for a period of 10 min: (a) Load versus tensile extension plot and (b) FESEM image of fracture surface.

The cracks were developed due to the brittle nature of the Ti_2Cu which shown by arrows in Figs 7b-11b. Fig. 7b and 9b showed that quasi-cleavage fracture appearance in the Ti-Ti matrix phase followed by brittle Ti_2Cu phase. Fig. 11 (b) indicated the quasi-cleavage major fractures of Ti included in the Ti_2Cu phase. Therefore, the fracture owing to quasi-cleavage is beneficial for the strength of the joint. The appearance of brittle fracture caused upon reduction of the strength of a bonded joint due to the formation of the intermetallic compound at the Ti/braze interface [17, 18, 30]. The main reasons for the crack initiation are the formation of the hard and brittle intermetallic compounds *viz*., Ti_2Cu, Ti_2Ni and/or Cu_2 (Ni, Zr) at Ti interface. Generally, the propagation of the cracks prefer at the brittle intermetallic compounds, which can spread easily through them during application of stress in tensile experiment [31]. The reduction of the strength of the joints and fracture behaviour upon propagation of the crack, which shows the morphological cleavage including facets characteristics. The measure of tensile strength and fracture behaviours demonstrated the appearance of the $NiTi_2$/Ti_2Cu/NiTi/Cu_2 (Ni,Zr), $(Ti, Zr)_2Ni$ and β(Ti, Zr) phases in the braze joints, which were detrimental and hence, they must be ignored in order to obtain a sound joint.

Preprints (www.preprints.org) | NOT PEER-REVIEWED | Posted: 21 June 2018 doi:10.20944/preprints201806.0328.v1

Conclusions

A. The typical representative plots of P-h obtained at a load of 5000μN for the (a) $Ti_{20}Zr_{20}Cu_{50}Ni_{10,}$ (b) $Ti_{20}Zr_{20}Cu_{40}Ni_{20,}$ (c) $Ti_{20}Zr_{20}Cu_{30}Ni_{30,}$ (d) $Ti_{20}Zr_{20}Cu_{20}Ni_{40}$ and (e) $Ti_{20}Zr_{20}Cu_{10}Ni_{50}$ metallic glasses with a view to understand the Hardness and Young's modulus properties of these metallic glasses. The present work is the very first experimental observation to the best of our knowledge, where density, nanoindentation at a constant peak load of 5000 μN, and the intrinsic contact resistance have been reported.

B. The nanomechanicals analysis for brazed samples of $Ti_{20}Zr_{20}Cu_{60-x}Ni_x$ (x=10, 20, 30, 40 and 50) metallic glasses with CP-Ti alloy were done. CP-Ti alloy pieces were respectively braze joined using metallic glass ribbon fillers of compositions (a) $Ti_{20}Zr_{20}Cu_{50}Ni_{10}$, (b) $Ti_{20}Zr_{20}Cu_{40}Ni_{20}$, (c) $Ti_{20}Zr_{20}Cu_{30}Ni_{30}$, (d) $Ti_{20}Zr_{20}Cu_{20}Ni_{40}$, and (e) $Ti_{20}Zr_{20}Cu_{10}Ni_{50}$ at 1263, 1240,1268, 1277 and 1279 K for a period of 10 min. (a) $(Ti, Zr)_2Cu$,Ti-rich, and α-Ti phases, (b) $NiTi_2$, Ti_2Cu , α-Ti and Ti-rich phases, (c) $NiTi_2$, Ti_2Cu , α-Ti and Ti-rich phases, (d) $NiTi_2$, $(Ti, Zr)_2Ni$,β (Ti, Zr) and Ti-rich phases and (e) $NiTi_2$, $Cu_2(Ni, Zr)$, NiTi ,α-Ti and Ti-rich phases in correspondence.

Acknowledgements

The authors gratefully acknowledge the support of this research through the fund provided by the University Grants Commission-Rajiv Gandhi National Fellowship (UGC-RGNF). AKB thanks the Indian National Science Academy (INSA), New Delhi India for the support through Senior Scientist Platinum jubilee Fellowship. The authors acknowledge the kind permission of Director, CSIR-Central Glass and Ceramic Research Institute, Kolkata 700032, India.

 doi:10.20944/preprints201806.0328.v1

Reference

1. Y. Zhao et al. Interfacial microstructure and mechanical properties of porous-Si3N4 ceramic and Ti-Al alloy joints vacuum brazed with Ag-Cu filler, Ceramics International 43 (2017) 9738–9745.
2. J. Cao, Xiangyu Dai, Jiaqi Liu, Xiaoqing Si, Jicai Feng, Relationship between microstructure and mechanical properties of TiAl/ Ti2AlNb joint brazed using Ti-27Co eutectic filler metal , Materials and Design 121 (2017) 176–184
3. Qiwen Qiu, Ying Wang, Zhenwen Yang, Xin Hu, Dongpo Wang, Microstructure and mechanical properties of TiAl alloy joints vacuum brazed with Ti–Zr–Ni–Cu brazing powder without and with Mo additive, Materials and Design 90 (2016) 650–659.
4. B.B. Medeiros et al. / Journal of Non-Crystalline Solids 425 (2015) 103–109.
5. M. Kazunari, I. Yuki, M. Hirotaka, and M. Hiroyuki: Scripta Mater, vol. 68, (2013), pp. 777–80.
6. X. L. Bian, G. Wang, K. C. Chan, J. L. Ren, Y. L. Gao, Appl. Phys. Lett. 103, 101907 (2013).
7. E. Ganjeh, H. Sarkhosh, M.E. Bajgholi, H. Khorsand, M.H. Ghaffari, Increasing Ti–6Al–4V brazed joint strength equal to the base metal by Ti and Zr amorphous filler alloys Materials characterization 71(2012)31-40.
8. Elrefaey A, Tillmann W. brazing of titanium to steel with different filler metals: analysis and comparison. J Mater Sci 45 (2010): 4332–8.

9. Lee JG, Choi YH, Lee JK, Lee GJ, Lee MK, Rhee CK. Low-temperature brazing of titanium by the application of a Zr–Ti–Ni–Cu–Be Bulk Metallic Glass (BMG) alloy as a filler. Intermetallics (2010); 18:70–3.

10. Y. Huang, Y.L. Chiu, J. Shen, J.J.J. Chen, J. Sun, Nanoindentation study of Ti-based metallic glasses, J. Alloys Compd. 479 (2009) 121–128.

11. Elrefaey A, Tillmann W. Correlation between microstructure, mechanical properties, and brazing temperature of steel to titanium joint. J Alloys Compd 487 (2009); 639–45.

12. N.K. Mukhopadhyay, A. Belger, P. Paufler, D.H. Kim, Nanoindentation studies on Cu–Ti–Zr–Ni–Si–Sn bulk metallic glasses, Mater. Sci. Eng. A 449–451 (2007) 954–957.

13. Y.J. Yang, F.W. Kang, D.W. Xing, J.F. Sun, Q.K. Shen, J. Shen, Formation and mechanical properties of bulk Cu–Ti–Zr–Ni metallic glasses with high glass forming ability, Trans. Nonferrous Met. Soc. China 17 (2007) 16–20.

14. Chang CT, Wu ZY, Shiue RK, Chang CS. Infrared brazing Ti–6Al–4V and SP-700 alloys using the Ti–20Zr–20Cu–20Nibraze alloy. Mater Lett (2007); 61:8425.

15. Materials Science International Team M. Ternary alloy systems: phase diagrams, crystallographic and thermodynamic data, V 11. Berlin, Germany: Springer; (2007).

16. Hong IT, Koo CH. Microstructural evolution and shears strength of brazing C103 and Ti–6Al–4V using Ti–20Cu–20Ni–20Zr (wt. %) filler metal. Int J Refract Met Hard Mater (2006); 24:247–52.

17. Doherty KJ, Tice JR, Szewczyk ST, Gilde GA. Titanium brazing for structures and survivability. Proceedings of the 3rdInternational Brazing and Soldering Conference; (2006). P. 268–73. San Antonio, Texas, USA.

18. N.K. Mukhopadhyay, P. Paufler, Micro- and nanoindentation techniques for a Mechanical characterization of materials, Int. Mater. Rev. 51 (2006) 209-245.

19. C.A. Schuh, T.G. Nieh, A survey of instrumented indentation studies on metallic glasses, J. Mater. Res. 19 (2004) 46–57.

20. W.C. Oliver, G.M. Pharr, Measurement of Hardness and Elastic Modulus by Instrumented Indentation: Advances in Understanding and Refinements to Methodology, J. Mater. Res. 19 (2004) 3-20.

21. Shiue RK, Wu SK, Chan CH. The interfacial reactions of infrared brazing Cu and Ti with two silver-based braze alloys.J Alloys Compd, 372, (2004); 148–57.

22. M. Calin, J. Eckert, L. Schultz, Improved mechanical behavior of Cu–Ti-based bulk metallic glass by in situ formation of nanoscale precipitates, Scr. Mater. 48 (2003) 653–658.

23. X.H. Lin, W.L. Johnson, Formation of Ti–Zr–Cu–Ni bulk metallic glasses, J. Appl. Phys. 78 (1995) 6514–6519.

 doi:10.20944/preprints201806.0328.v1

24. H. Choi-Yim, R. Busch, W.L. Johnson, The effect of silicon on the glass forming ability of the Cu47Ti34Zr11Ni8 bulk metallic glass forming alloy during processing of composites, J. Appl. Phys. 83 (1998) 7993–7997.

25. M J Donachie. Titanium: a technical guide. 2 ed. USA: ASM; (2000).

26. Chang E, Chen CH. Low-melting-point titanium-base brazing alloys—part 2: characteristics of brazing Ti.21Ni–14Cu on Ti–6Al–4V substrate. JMEPEG (1997); 6:797–803.

27. Metals hand book, vol 3: alloy phase diagrams. ASM; (1992).

28. Schwartz MM. Brazing. 2 ed. USA: ASM; (2003).

29. Dieter GE. Mechanical metallurgy. 3 ed. USA: McGraw Hill; (2001).

30. Oliver W. C. and Pharr G. M., J. Mater. Res. 7 (1992) 1564.

31. JIS Z 3192. Methods for tension and shear tests for brazed joint; 1988.